



PCCP

**Dissolution kinetics of a sodium borosilicate glass in Tris buffer solutions: Impact of Tris concentration and acid (HCl/HNO<sub>3</sub>) identity**

Journal:	<i>Physical Chemistry Chemical Physics</i>
Manuscript ID	CP-ART-12-2020-006425.R1
Article Type:	Paper
Date Submitted by the Author:	18-Jun-2021
Complete List of Authors:	Stone-Weiss, Nicholas; Rutgers The State University of New Jersey, Materials Science and Engineering Smith, Nicholas; Corning Inc, Science and Technology Division Yougman, Randall; Corning Inc, Science and Technology Division Pierce, Eric; Oak Ridge National Laboratory, Environmental Sciences Division Goel, Ashutosh; Rutgers The State University of New Jersey, Materials Science and Engineering

SCHOLARONE™  
Manuscripts

Dissolution kinetics of a sodium borosilicate glass in Tris buffer  
solutions: Impact of Tris concentration and acid (HCl/HNO<sub>3</sub>) identity

Nicholas Stone-Weiss,<sup>1</sup> Nicholas J. Smith,<sup>2</sup> Randall E. Youngman,<sup>2</sup> Eric M.

Pierce,<sup>3</sup> Ashutosh Goel<sup>1,\*</sup>

<sup>1</sup>Department of Materials Science and Engineering, Rutgers, The State University of New Jersey,  
Piscataway, NJ 08854, United States

<sup>2</sup>Science and Technology Division, Corning Incorporated, Corning, NY 14831, United States

<sup>3</sup>Environmental Sciences Division, Oak Ridge National Laboratory, Oak Ridge, TN 37831,  
United States

---

\* Corresponding author:  
Email: [ag1179@soe.rutgers.edu](mailto:ag1179@soe.rutgers.edu); Ph: +1-848-333-1523

## Abstract

Understanding the corrosion behavior of glasses in near-neutral environments is crucial for many technologies including glasses for regenerative medicine and nuclear waste immobilization. To maintain consistent pH values throughout experiments in the pH = 7 to 9 regime, buffer solutions containing tris(hydroxymethyl)aminomethane (“Tris”, or sometimes called THAM) are recommended in ISO standards 10993-14 and 23317 for evaluating biomaterial degradation and utilized throughout glass dissolution behavior literature—a key advantage being the absence of dissolved alkali/alkaline earth cations (i.e. Na<sup>+</sup> or Ca<sup>2+</sup>) that can convolute experimental results due to solution feedback effects. Although Tris is effective at maintaining the solution pH, it has presented concerns due to the adverse artificial effects it produces while studying glass corrosion, especially in borosilicate glasses. Therefore, many open questions still remain on the topic of borosilicate glass interaction with Tris-based solutions. We have approached this topic by studying the dissolution behavior of a sodium borosilicate glass in a wide range of Tris-based solutions at 65 °C with varied acid identity (Tris-HCl vs. Tris-HNO<sub>3</sub>), buffer concentration (0.01 M to 0.5 M), and pH (7-9). The results have been discussed in reference to previous studies on this topic and the following conclusions have been made: (i) acid identity in Tris-based solutions does not exhibit a significant impact on the dissolution behavior of borosilicate glasses, (ii) ~0.1 M Tris-based solutions are ideal for maintaining solution pH in the absence of obvious undesirable solution chemistry effects, and (iii) Tris-boron complexes can form in solution as a result of glass dissolution processes. The complex formation, however, exhibits a distinct temperature-dependence, and requires further study to uncover the precise mechanisms by which Tris-based solutions impact borosilicate glass dissolution behavior.

## Keywords

Borosilicate, Solution chemistry, Corrosion, Buffer

## 1. Introduction

Understanding the corrosion behavior of silicate glasses in aqueous solutions is imperative for nearly all technological applications, as chemical durability has always been one of the prerequisites when deciding the suitability of a glass composition for its final application. Whether developing glasses with controlled dissolution kinetics for application in regenerative medicine or glasses with high durability for the immobilization of nuclear waste, a thorough understanding of their dissolution behavior as a function of the experimental conditions is mandatory for the successful design of glass compositions for functional applications.

The existing literature on glasses for regenerative medicine or nuclear waste containment typically utilizes solutions containing tris(hydroxymethyl)aminomethane (“Tris”, or sometimes called THAM) coupled with an inorganic acid as a buffering solution to model their aqueous corrosion in the neutral-to-alkaline environments ( $\text{pH} = 7\text{-}9$ ) likely to be encountered for these applications. For example, ISO standards 10993-14<sup>1</sup> and 23317<sup>2</sup> describe the methodologies necessary to evaluate the behavior of biomaterials in simulated body conditions, with the former recommending the use of a Tris-HCl buffer at  $\text{pH} = 7.4$  to measure the degradation behavior of bioactive glasses and ceramics, and the latter recommending using Tris-HCl to prepare simulated body fluid (SBF) for evaluating apatite-forming ability on the surface of biomedical implants. Accordingly, the published literature on bioactive glasses utilizes predominantly these two standards, thus implementing different compositions of Tris-based buffer solutions to assess their *in vitro* bioactivity. Further, in the field of nuclear waste immobilization, ASTM C1220-17<sup>3</sup> defines the test parameters necessary to evaluate the static aqueous corrosion behavior of potential monolithic waste forms, stating that the leachate solutions can consist of buffered or non-buffered solutions to study different facets of glass corrosion behavior. As a result, several studies exploring the corrosion behavior of glass, either for nuclear waste,<sup>4</sup> or other technological applications,<sup>4-20</sup>

utilize experimental methodologies involving Tris-based buffer solutions (in varying concentrations) to ensure pH stability throughout experiments and extract dissolution kinetics. Despite the demonstrated widespread use and benefits of utilizing Tris-based buffer solutions, Tris additions can also create adverse effects upon corrosion behavior which have, until now, been largely ignored or unverified. The benefits and drawbacks of utilizing Tris as a buffer have been highlighted below.

As a brief reminder to the reader, Tris is a weak base with a  $pK_b$  of 5.92 at 25 °C. The corresponding  $pK_a$  of its conjugate acid ( $\text{TrisH}^+$ ) is 8.08, thus indicating an ideal buffering range ( $pK_a \pm 1$ ) between pH 7-9,<sup>21</sup> which is close to neutral as well as physiological conditions of interest. Preparations of buffer solutions based on Tris are commonly achieved by additions of strong acids (such as HCl or  $\text{HNO}_3$ ) to aqueous solutions containing Tris at the desired molarity, which is chemically equivalent to Tris being mixed with its corresponding  $\text{TrisH}^+$  salt—the latter at the same molar concentration as the strong acid added to the aqueous solution. Tris buffer is particularly attractive for dissolution experiments since its solutions do not require dissolved alkali/alkaline earth cations (i.e.  $\text{Na}^+$  or  $\text{Ca}^{2+}$ ) that can convolute experimental results due to solution feedback effects.<sup>22</sup> For instance, the presence of  $\text{Na}^+$  in the contact solution will not only affect its ionic strength but will also slow down the process of chemical dissolution by shifting the equilibrium of the ion exchange reaction ( $\equiv\text{Si}-\text{O}-\text{Na} + \text{H}_3\text{O}^+ \rightleftharpoons \equiv\text{Si}-\text{OH} + \text{Na}^+ + \text{H}_2\text{O}$ ) towards the left in Na-containing glasses.<sup>22, 23</sup> Further, Jollivet et al. have determined that the presence of anions in solution (i.e.  $\text{Cl}^-$ ,  $\text{SO}_4^{2-}$ ) has comparatively smaller effects on dissolution rates as compared to dissolved metal cations.<sup>24</sup> Despite this finding, the absence of dissolved metal cations does not in and of itself ensure straightforward data interpretation, given that organic molecules (Tris included) have also been observed to create adverse artificial effects when in contact with glass.<sup>25-32</sup>

Concerns with Tris-based buffer solutions were initially raised in bioactive glass literature, as accelerated kinetic effects (at least 2×) were observed for bioactive glasses and glass-ceramic scaffolds exposed to Tris-based and/or SBF-Tris-based solutions as compared to analogous samples exposed to Tris-free conditions, due to selective leaching and surface complexation caused by the Tris component.<sup>26, 27</sup> Further, more recent studies have suggested that the acid used in Tris-based leaching solutions can also impact the extent of bioactive glass degradation and surface layer characteristics.<sup>30, 33</sup> Given these concerns, alternative buffer solutions have been explored as potential replacements for Tris while assessing *in vitro* bioactivity; however, alternative buffers added to SBF have produced similar or worse effects as Tris-SBF to accelerate material degradation and alter the rate of apatite-layer formation.<sup>28, 29</sup> Thus, at present, Tris is still regarded as the most suitable buffer solution for assessing biomaterial responses *in vitro*. Until now, the adverse effects discussed for Tris-based solutions have only considered silicate glass and glass-ceramic chemistries (also containing small fractions of P<sub>2</sub>O<sub>5</sub>), while borosilicate glass compositions—which are candidates for the design of novel third-generation biomaterials and are also instrumental for nuclear waste containment—have not been considered. However, borosilicate compositions show particularly significant adverse effects,<sup>25</sup> as discussed below.

The dissolution kinetics of borosilicate glasses has been shown to accelerate by as much as 8× when in contact with Tris-containing solutions as compared to Tris-free solutions, as observed by Tournié et al.<sup>25</sup> Comparing dissolution behavior between a soda-lime silicate glass and a sodium borosilicate glass revealed that this significant increase in dissolution rate in Tris-based media was not observed for the former, while the latter exhibited a substantial dissolution rate elevation in both Tris-HCl and Tris-HNO<sub>3</sub> environments, although to a more pronounced extent in Tris-HCl.<sup>25</sup> Such a rapid acceleration of dissolution kinetics was attributed to the formation of Tris-boron complexes (at 1:1 stoichiometry), which—while still not fully understood—was assumed to occur either by (i)

complexation of boron with Tris in the solution, or (ii) by adsorption of Tris molecules on boron sites at the glass surface, thus increasing the rate of boron release and causing more rapid hydrolysis of the surrounding glass network.<sup>25</sup> Wesolowski et al. observed such a complexation effect to significantly increase the solubility of Al in the presence of bis-Tris ions, but not in the presence of Tris itself.<sup>34</sup> Since Tris-based solutions have been shown to exhibit such a large impact on borosilicate degradation kinetics, it is of vital importance to understand the mechanisms by which Tris affects glass dissolution behavior, especially to aid in selecting aqueous media adequate to study and accurately predict the dissolution behavior of borosilicate glasses.

Borosilicate glasses are utilized in many critical glass technologies that require a thorough understanding of glass corrosion behavior in near-neutral conditions.<sup>16, 35-38</sup> Therefore, it will be ideal to uncover the science governing Tris-glass interactions for designing solutions which minimally impact the dissolution kinetics of borosilicate glasses. As has been discussed previously, although alternative buffer solutions have been investigated, the present consensus in the glass community is that Tris-based solutions are the best choice while studying the near-neutral pH regime since these solutions provide the required pH stability in the absence of dissolved metal cations which can adversely affect dissolution kinetics. Presented with this challenge, and considering previous literature on this topic, the focus of the present study is to re-evaluate the magnitude and mechanisms by which Tris buffer solutions may affect the apparent dissolution behavior of borosilicate glasses, particularly aiming to address the following open questions/inconsistencies observed in the literature: (1) How does the identity of the acid in Tris-based buffer solution impact the dissolution behavior of a borosilicate glass? (2) How are the dissolution kinetics of a borosilicate glass affected by varying the Tris-to-acid ratio in the solution? and (3) Is there a measurable effect that manifests as a function of the concentration of Tris in solution at fixed pH? Accordingly, the present study focuses on the dissolution behavior of a

sodium borosilicate glass in Tris-based (pH = 7-9) solution environments with varied Tris concentrations (0.01 – 0.5 M) and acid identities (HCl vs. HNO<sub>3</sub>). Included in this pursuit are experiments to interrogate the underlying physical mechanisms by which glass degradation kinetics are influenced, especially by examination of whether Tris-boron complexation occurs on the surface or in solution.

## 2. Experimental

### 2.1 Synthesis of the glass

A sodium borosilicate composition (25 Na<sub>2</sub>O–25 B<sub>2</sub>O<sub>3</sub>–50 SiO<sub>2</sub>; in mol.%) was synthesized via the melt-quench technique, using high-purity powders of SiO<sub>2</sub> (Alfa Aesar; >99.5%), H<sub>3</sub>BO<sub>3</sub> (Alfa Aesar; ≥98%), and Na<sub>2</sub>SiO<sub>3</sub> (Alfa Aesar; >99%) as precursors. Oxide precursors were mixed in a 70 g batch and melted in a Pt-Rh crucible for 90 minutes in air at 1450 °C. The glass melt was quenched on a metallic plate and coarse-annealed at a temperature of T<sub>g</sub><sup>\*</sup>-50 °C, where T<sub>g</sub><sup>\*</sup> is the estimated glass transition temperature as obtained from the SciGlass database.<sup>39</sup> The amorphous nature of the glass sample was confirmed by X-ray diffraction (XRD) (PANalytical – X'Pert Pro; Cu K<sub>α</sub> radiation; 2θ range: 10–90°; step size: 0.01313° s<sup>-1</sup>). The actual concentration of SiO<sub>2</sub> and B<sub>2</sub>O<sub>3</sub> in the synthesized glasses was determined by ICP–OES (PerkinElmer Optima 7300V), while sodium concentration was determined by flame emission spectroscopy (Perkin Elmer Flame Emission Analyst 200).

### 2.2 Glass transition temperature measurements and annealing

Differential scanning calorimetry (DSC) data were collected on fine glass powders (<45 μm diameter) using a Simultaneous Thermal Analyzer (STA 8000; PerkinElmer) from room temperature to 1500 °C at a heating rate of 20 °C/min under a constant flow of nitrogen gas. The glass transition

temperature ( $T_g$ ) was deduced from the inflection point of the endothermic dip in the DSC traces, where the reported  $T_g$  is the average value from three thermal scans. After experimental  $T_g$  measurements, the glass was re-annealed for several hours at a temperature corresponding to  $T_g-50$  °C and slow-cooled to room temperature until most of the residual stresses were removed, as visualized under a polariscope. A more detailed description of the method used to anneal the glasses has been described in our previous article.<sup>35</sup>

### ***2.3 Bulk structural analysis of the as-synthesized and post-dissolution glass samples***

The structure of glass—both before and after chemical dissolution experiments—has been studied using  $^{11}\text{B}$  MAS NMR spectroscopy. The spectra were acquired using a commercial spectrometer (VNMRs, Agilent) and a 3.2 mm MAS NMR probe (Agilent). The samples were powdered in an agate mortar, packed into 3.2 mm zirconia rotors, and spun at 20 kHz. Experiments were conducted at 16.4 T (224.52 MHz resonance frequency), incorporating a 4 s recycle delay, short radio frequency pulses (0.6  $\mu\text{s}$ ) corresponding to a  $\pi/12$  tip angle, and signal averaging of 400 to 1000 scans. The acquired spectra were processed with minimal apodization and referenced to aqueous boric acid (19.6 ppm). Fitting of the MAS NMR spectra was performed using DMFit.<sup>40</sup> The “Q MAS  $\frac{1}{2}$ ” and Gaus/Lor functions were used to fit 3- and 4-fold coordinated boron resonances in the  $^{11}\text{B}$  MAS NMR data, respectively, and  $N_4$  was calculated from the relative areas of these peaks, with a small correction due to the overlapping satellite transition of the 4-fold coordinated boron peak.<sup>41</sup>

### ***2.4 Chemical durability of glasses***

#### ***2.4.1 Surface area analysis of glass powder specimens***

The studied glass was crushed and sieved to obtain powders with particle sizes varying between 300 – 425  $\mu\text{m}$ . The glass particles were ultrasonically washed in acetone to remove any fine powder residue adhering to the surface of larger particles. This process was repeated at least

three times, or until the supernatant was clear, to ensure the removal of all fine particles. The ultrasonically washed glass particles were dried overnight at room temperature in ambient air and analyzed for any structural changes before versus after acetone-washing using Fourier Transform Infrared (FTIR) spectroscopy. The IR spectra were acquired using a single-bounce diamond attenuated total reflectance (ATR) apparatus (FTIR-UATR, Frontier™, PerkinElmer, Inc.; scanning resolution  $4\text{ cm}^{-1}$ , 32 scans for background and samples). The average three-dimensional (3D) geometric surface area of washed particles was determined using ImageJ software (as explained in more detail in Ref.<sup>35</sup>) after capturing images of  $\sim 1000$  particles via an optical microscope (Zeiss Axioskop 40) at  $\sim 50X$  magnification. Experimental density values (measured using Archimedes' method by measuring the mass of sample in air and d-limonene solution; number of samples = 3, standard deviation  $< 0.009\text{ g cm}^{-3}$ ) were used together with 3D surface area calculations to determine the specific surface area of the washed powders ( $\sim 4100\text{ mm}^2/\text{g}$ ). Finally, the mass of glass particles resulting in the desired surface area-to-volume ratio (SA/V) was calculated.

#### *2.4.2 Dissolution behavior and kinetics of glass corrosion*

The dissolution behavior and corrosion kinetics of glasses was studied in Tris-HCl and Tris-HNO<sub>3</sub> solutions with pH = 7, 8, and 9. In each experiment, 30.0 mg of acetone-washed glass particles was immersed in 50 mL of solution, corresponding to  $\text{SA/V} = 2.5\text{ m}^{-1}$ . Solutions with initial pH buffered to either 7 or 9 were prepared at concentrations of 0.1 M Tris, whereas solutions with pH = 8 were prepared at Tris concentrations of 0.01, 0.05, 0.1, 0.3, and 0.5 M to examine concentrative effects. Each combination of solution pH and Tris concentration mentioned above was duplicated using both HCl and HNO<sub>3</sub> as the acid in the buffer solution—hereafter referred to as either Tris-HCl or Tris-HNO<sub>3</sub>. Solutions were prepared by dissolving the required amount of Tris in deionized (DI) water and adjusting the pH to the desired value with 1 M solutions of either HCl or HNO<sub>3</sub>. The final buffer solutions were prepared within  $\pm 0.02$  of the target pH (at room temperature;

hereafter assumed to be 25 °C), in batches with a total volume of  $2 \pm 0.05$  L to maintain accurate Tris molarity in the solution. All powder–solution mixtures were immediately sealed into sterilized polypropylene flasks and placed in an oven at 65 °C. Experiments ranged from 15 minutes to 24 hours. In addition to analyses of neat (unused) and blank (glass-free) control solutions, all experiments were performed three times to evaluate uncertainty in final results. The pH of each solution recovered from experiments was measured at room temperature using a pH meter (Mettler Toledo InLab® Pro-ISM). Separate aliquots of recovered solutions were chemically analyzed by ICP-OES (PerkinElmer Optima 8300). ICP-OES detection limits were  $<0.5$  ppm for Na,  $<0.2$  ppm for B, and  $<0.2$  ppm for Si. The normalized loss (NL) of glass on the basis of each element (Na, B, and Si) released into the surrounding solution was calculated using equation (1),

$$NL_i = \frac{C_i - C_o}{\left(\frac{SA}{V}\right) f_i} \quad (1)$$

where  $C_i$  is the mass concentration of element  $i$  in the solution as detected by ICP-OES;  $f_i$  is the mass fraction of the element  $i$  in the glass;  $C_o$  is the background concentration (as determined from blank solutions). Normalized loss data were plotted against time and linearly fit over the apparent linear regimes of release at early times to estimate the forward dissolution rates for each element in the glass and solution environment studied.

To further evaluate the mechanisms of glass degradation, solution and bulk structural characterization of pre- and post-dissolution glass specimens were performed. For the examination of dissolved structural species, selected liquid aliquots were studied using  $^{11}\text{B}$  solution NMR. These experiments were performed at 11.7 T (160.46 MHz resonance frequency), incorporating a 1 s recycle delay,  $\pi/4$  tip angle pulses, and signal averaging over at least 1000 scans. These experiments were performed at 25 °C (room temperature) and 65 °C (to reproduce the *in situ* dissolution temperature). The spectra of recovered liquid aliquots were also compared to that of a reference

sample, which was utilized to identify the chemical shifts of potential dissolved borate species (i.e.  $\text{H}_3\text{BO}_3$  and Tris-boron complexes). This sample was prepared according to the procedure described by Tournié et al.<sup>25</sup>: two solutions were mixed in a 1:1 ratio—(i) a solution of 0.1 M  $\text{H}_3\text{BO}_3$ , achieved by dissolving  $\text{H}_3\text{BO}_3$  powder (Alfa Aesar;  $\geq 98\%$ ) in DI water and adjusting the pH to 8 with 1 M NaOH, and (ii) 0.1 M Tris-HCl (pH = 8), prepared according to the procedures described above. The selected 1:1 mixture (equivalent to a Tris/B ratio equal to 1) was chosen since it displayed maximum signal from Tris-boron complexes in Ref.<sup>25</sup>

For bulk analyses following glass dissolution, the recovered glass powders were rinsed thoroughly with DI water three times and then submerged in ethanol (Fisher Chemical, anhydrous) to (i) facilitate drying the samples at room temperature and (ii) effectively cease glass-water reactions near the glass surface. The samples were then characterized using XRD and  $^{11}\text{B}$  MAS NMR spectroscopy.

#### *2.4.3 Surface characterization of dissolved monolithic coupons*

To further understand the surface chemistry of the dissolved samples, similar tests were performed on monolithic glass coupons at pH = 7 in 0.1 M Tris-HCl and Tris- $\text{HNO}_3$  solutions submerged for 24 hours. Accordingly, three coupons with the dimensions  $\sim 10\text{ mm} \times \sim 10\text{ mm}$  were cut for the studied glass composition using a diamond blade, with one sample serving as a polished (non-corroded) control sample. The polishing of the glass coupons was performed according to the procedure described in ASTM C1220-17,<sup>3</sup> where the glass samples were ground in acetone sequentially using 120 – 600 grit sized SiC sheets followed by polishing in 6  $\mu\text{m}$  and 3  $\mu\text{m}$  non-aqueous diamond suspensions until a mirror finish was acquired. The thickness of the polished samples was  $\sim 1\text{ mm}$ . The dimensions of the rectangular polished samples were measured to calculate the geometric surface areas. The glass coupons were hereafter subjected to identical

dissolution conditions ( $65\text{ }^{\circ}\text{C}$ ,  $\text{SA/V} = 2.5\text{ m}^{-1}$ ) and drying procedure as has been described for powders in *section 2.4.2*.

X-ray photoelectron spectroscopy (XPS) measurements on monolithic glass coupons were performed to understand the chemical composition within the top 5-10 nm of polished and dissolved sample surfaces. The XPS measurements utilized a Thermo Scientific K-Alpha equipment, which used a 1486.6 eV monochromated Al  $\text{K}_{\alpha}$  x-ray source to excite core level electrons from the sample. A low energy dual electron/argon-ion beam flood gun was used for charge compensation during measurements. The kinetic energy of the photoelectrons was measured using a  $180^{\circ}$  double-focusing hemispherical analyzer with a 128-channel detector. The binding energy scale was referenced to the main component of the adventitious C 1s peak positioned at 284.8 eV. The photoelectron spectrometer was calibrated using the Au $4f_{7/2}$  binding energy (83.96 eV) for the etched surface of the Au metal reference. The analyzer was operated in the constant resolution mode with a pass energy of 10 eV for high-resolution spectroscopy, while a pass energy of 50 eV was used for the routine survey scans. Peak areas were fitted using Gaussian/Lorentzian functions and the peak areas were converted to composition using suitable elemental relative sensitivity factors<sup>42</sup> and corrected for attenuation through an adventitious carbonaceous overlayer using a calculation similar to the method described by Smith.<sup>43</sup> The probe depth of XPS, taken to be three times the inelastic mean free path of photoelectrons, was 3.6 nm for Na 1s, 6.9 nm for O 1s, and 9.3 nm for B 1s and Si 2p.

The hydrogen profiles on the surface of polished and dissolved samples were determined by elastic recoil detection analysis (ERDA) using a 2.0 MeV  $\text{He}^{++}$  beam (General Ionex Tandatron accelerator). The beam was oriented in a grazing geometry with an angle of  $75^{\circ}$  between the incident beam and the surface normal. The detector was mounted at  $75^{\circ}$  with respect to the surface normal in the specular direction, with a 40  $\mu\text{m}$  mylar foil placed over the active area to block

scattered He ions. Hence, only forward-scattered H ions were able to penetrate the detector. The probe depth of ERDA is approximately 350 nm.

### 3. Results

#### 3.1 Glass formation behavior and bulk properties

The as-synthesized glass sample was transparent in appearance and determined to be amorphous via XRD analysis (as shown in Figure S1). The experimentally measured glass composition (25.2 Na<sub>2</sub>O–25.0 B<sub>2</sub>O<sub>3</sub>–49.8 SiO<sub>2</sub>; mol.%) is in very close agreement with the batched target composition (within ±0.2 mol.%). T<sub>g</sub> and density were measured as 565±6 °C and 2.487±0.003 g/cm<sup>3</sup>, respectively, which both agree well with the literature on similar compositions.<sup>44</sup> After analyzing the annealed glass under a polariscope, it was estimated to have less than 10 MPa of remaining residual stresses, as calculated from its ~5 mm sample thickness and considering the absence of first-order fringes under cross-polarized light.

#### 3.2 Structural analysis of glasses

Figure 1 presents the <sup>11</sup>B MAS NMR spectra and fitted peaks for the studied glass. This spectrum displays two main resonances: a broad peak centered near 15 ppm associated with trigonal boron species (BO<sub>3</sub>) and a strong, relatively narrow peak centered near 0 ppm associated with tetrahedral boron species in the glass (BO<sub>4</sub>). The trigonal boron peak contains contributions from both ring and non-ring species, where ring species exhibit downfield shifts as compared to non-ring species (18.5 vs. 16.2 ppm in the fitted spectra, respectively).<sup>45</sup> The tetrahedral boron peak consists of resonances likely associated with fully polymerized BO<sub>4</sub> units with bridging oxygen (BO) to either 3Si/1B or 4 Si. The former unit is typically shifted downfield from the latter, as evidenced by the 0.0 vs. -1.9 ppm chemical shifts in the fitted spectrum.<sup>45</sup> The measured *N*<sub>4</sub> fraction (percentage of BO<sub>4</sub> species) in the studied glass is 68.2%, where each BO<sub>4</sub><sup>-</sup> unit requires charge compensation by Na<sup>+</sup> in the glass. Using this result in combination with the Dell, Yun, and Bray model,<sup>46-48</sup> the

silicate network is calculated to include 67.3% fully polymerized  $Q^4$  units ( $Q^n$ , where  $n$  is the number of BO per Si tetrahedron), with the remainder being  $Q^3$  units with 1 non-bridging oxygen (NBO) charge-balanced by the remaining  $\text{Na}^+$  in the glass. Based upon the calculated R (Na/B) and K (Si/B) values (1.01 and 1.99, respectively) and considering a threshold value of  $R \approx 1$  from Dell et al.,<sup>48</sup> NBOs are expected to exist predominantly on silicate species while only negligible fractions of anionic  $\text{BO}_3$  species containing 1 NBO are expected. The glass structural characteristics will be revisited in the next section as structural evolution upon glass dissolution will likewise be assessed by  $^{11}\text{B}$  MAS NMR.

### **3.3 Chemical dissolution behavior**

#### *3.3.1 Buffering capacity of Tris-solutions as a function of glass dissolution kinetics*

The pH readings for all the dissolution experiment durations and solution environments are presented in Table S1. Figure 2 graphically depicts the spread of pH data in solutions with initial pH = 8, as a function of the Tris molarity in solution. Further, Figure S2 displays the pH vs. time curves for all the Tris-HCl and Tris- $\text{HNO}_3$  solutions investigated in the present study, organized according to the starting pH and Tris molarity. As the oxide glass network dissolves—particularly when released in proportions congruent with the parent glass composition—the release of Na and B into solution (along with O from the network) can be thought of as tantamount to the corresponding release of  $\text{Na}_2\text{O}$  (with  $\text{H}_2\text{O} \rightarrow 2 \text{NaOH}$ , i.e., sodium hydroxide) and  $\text{B}_2\text{O}_3$  (with  $\text{H}_2\text{O} \rightarrow \text{H}_3\text{BO}_3$ , i.e., boric acid). In this way, the apparent release of  $\text{Na}^+$  tends to increase solution pH, while the dissolution of B from the glass behaves like an increase in boric acid in solution and reduces the surrounding solution pH. The impact that these dissolved species have upon final solution pH will of course follow the chemical equilibrium established with the Tris-related buffering species in solution, wherein the ability for a buffer to resist pH change when acidic or basic species are added to the solution is referred to as buffering capacity. In our studies at pH = 8, it is observed that with

sufficiently concentrated Tris molarities in the range of 0.1 to 0.5 M, the pH in solution stays largely constant for up to 24 h of glass submersion, and wherein the spread in pH does not change by more than +0.1 ( $\sim 8.0$ - $8.1$ ). At lower Tris concentrations in the range of 0.01 and 0.05 M, the buffering capacity of the solution is reduced to the point that pH changes by as much as +0.6 and +0.2 ( $\sim 8.0 \rightarrow 8.6$  and  $\sim 8.0 \rightarrow 8.2$ ), respectively, over the course of 24 h with the glass being used in the present study. Similar pH evolution behavior is observed regardless of the acid identity, i.e., Tris-HCl vs. Tris-HNO<sub>3</sub> solutions both behaved comparably. In pH = 7 and 9 solutions (all at 0.1 M Tris concentration), pH was observed to vary by less than +0.2 and  $\pm 0.1$ , respectively, regardless of the acid identity in the solution or the duration of glass submersion. Thus, as expected, higher concentrations of Tris in solution generally lead to enhanced buffering capacity from the pH-influencing elements released into solution from the glass. At fixed concentration (0.1 M Tris), solutions prepared at pH = 7 do not appear to buffer as well compared to those at pH = 8 or 9, as displayed in Figure S2. This observation is counterintuitive, as Tris buffer solutions at pH = 7 should, in theory, have greater buffering capacity against shifts to alkaline pH than solutions at pH = 8 or 9; here, the apparently greater shift in pH can instead be attributed to the greater total concentration of alkali (Na) released from the glass in pH = 7 vs 8 or 9 over the same experimental timeframe.

### *3.3.2 Elemental release behavior of glass in varied solution environment*

All the elemental concentrations and normalized mass loss (NL) data are presented in Table S1. As the glass is brought in contact with Tris-based solutions (pH = 7-9), ion exchange and hydrolysis promote rapid, linear increases in NL with time (forward rate regime). This is followed by concave downward behavior and transition into the residual rate regime, in which release rates slow to the point that dissolution and re-condensation reactions occur in tandem and produce a minimized, quasi-steady-state release rate. The absence of a true thermodynamic equilibrium

between glass and solution stems from the non-equilibrium nature of the glassy state, which will spontaneously dissolve in water due to a perpetual chemical potential gradient across the glass–fluid interface and allow for continued release over time. The transition from forward to residual rate is specifically attributed to the following: the development of secondary phases near the glass surface (i.e., gel/precipitate layer) and/or solution feedback effects as dissolved species approach saturation limits in the surrounding solution.<sup>23, 49, 50</sup>

Figure 3a-c displays NL vs. time curves depicting the dissolution behavior of the glass under investigation in the 0.1 M Tris-HNO<sub>3</sub> solutions at pH = 7 (Figure 3a), 8 (Figure 3b), and 9 (Figure 3c). The Na and B exhibit a nearly identical release behavior from the glass, while the NL curve for Si lies significantly below that of Na and B. A similar trend has been observed in all the studied solutions, regardless of their initial characteristics (chemistry and pH). We will next compare both the initial dissolution behavior and the transition towards residual rate behavior for this glass in the varied solution chemistries explored, specifically comparing the impacts of (i) Tris concentration, (ii) acid identity, and (iii) starting solution pH. Given that the static experiments performed in the present investigation were performed in dilute conditions at low SA/V, a reasonable estimation of the forward rate behavior can be made;<sup>51</sup> however, in the absence of stirring or replenishment of effluent solution, the rate determined is still an estimate of the “true” forward rate. Further, the present experiments do not reach a “true” residual rate behavior due to the low SA/V and short time durations of our experiments. For this reason, the following discussion refrains from emphasizing true “forward rate” or “residual rate” behavior, since the behavior witnessed in the present investigation is likely in between each of these kinetic regimes.

### 3.3.2.1 Impact of Tris concentration on the dissolution behavior of glass

Figure 4 presents the impact of Tris molarity (0.01 M – 0.5 M) and acid identity (HCl vs. HNO<sub>3</sub>) on the normalized release of boron (as a function of dissolution time) from the glass into the

solutions at pH = 8. As is evident, an increase in the concentration of Tris in the solution results in slower dissolution kinetics of the borosilicate glass, albeit not always in discernible orders of concentration (within experimental uncertainty). For instance, after 24 h, the NL of boron ( $NL_B$ ) from the glass into the solutions (both Tris-HCl – Figure 4a and Tris-HNO<sub>3</sub> – Figure 4b) with 0.01 M Tris concentration has been measured to vary between 215-250 g/m<sup>2</sup>, while its value is as low as 125-140 g/m<sup>2</sup> in the solutions containing 0.5 M Tris—a reduction in the NL by a factor of ~2. Similar suppression can be observed in the release behavior of Na and Si from the glass into the solutions with an increase in the concentration of Tris from 0.01 to 0.5 M, as discussed below.

To better quantify the impact of Tris concentration on the forward rate behavior, linear regression has been performed on the elemental NL data obtained during the first 3 h of glass dissolution. The rates extracted from the slopes of the fitted curves, which represent an estimated forward rate, are depicted in Figure 5, while rate values can be found in Table 1. The error bars displayed in the plot have been calculated from the uncertainty in the least-squares fitting method (discussed by Kragten<sup>52</sup>) using a similar approach as described in our previous publication.<sup>53</sup> A general decrease in the dissolution rates is observed for all the elements being released from the glass with increasing Tris concentration in the solution, where these decreases are particularly evident in the contrast of Na and B rates between low Tris concentrations (0.01–0.1 M) and high Tris concentrations (0.3–0.5 M). For instance, the rates for Na in the solutions with 0.01 M and 0.5 M Tris-HCl have been determined as ~30 and ~15 g m<sup>-2</sup> h<sup>-1</sup>, respectively. The dissolution rates remained at least 2× higher for Na and B as compared to Si in all the pH = 8 solutions. The suppression of the magnitude of elemental release from the glass into the solutions containing higher Tris concentrations (particularly for 0.3 M and 0.5 M solutions), as observed in both the initial dissolution regime and in the transition into the residual rate regime, is likely associated either with (i) a reduction of the rate of dissolution mechanisms (i.e., ion exchange/hydrolysis) due

to solution feedback effects, or (ii) modifications in the rate of formation or characteristics of a surface gel layer. This topic will be revisited in the discussion section.

### 3.3.2.2 Impact of acid identity upon glass dissolution behavior

Figures S3(a-c) present a comparison between the normalized release of B and Si from the glass into Tris-HCl and Tris-HNO<sub>3</sub> solutions at pH = 7, 8, and 9, respectively. Given the close overlap in the NL curves—especially in the forward rate regime—and considering the 15-25% errors typically associated with performing static dissolution experiments,<sup>51, 54, 55</sup> it is evident that the acid identity in the Tris buffer solution has an insignificant impact on the dissolution behavior of borosilicate glass. A comparison of the dissolution rates in Tris-HCl and Tris-HNO<sub>3</sub> solutions can be extracted from Figures 5 and 6, and Table 1. It is noteworthy that in pH = 8 solutions with  $\geq 0.1$  M Tris, HCl- and HNO<sub>3</sub>-based solutions with equimolar concentrations show a close overlap (within  $\pm 10\%$ ) in the NL rates calculated for Na, B, or Si. On the other hand, in the solutions with  $< 0.1$  M Tris, up to 15-20% reduction is observed for Tris-HNO<sub>3</sub> dissolution kinetics as compared to Tris-HCl. These disparities at low Tris concentrations, which may be attributed to the experimental uncertainty, can likewise be explained by the pH drift of the surrounding solution (i.e., the differences between otherwise identical Tris-HCl and Tris-HNO<sub>3</sub> solutions), since the aforementioned solutions do not buffer as well as those with  $\geq 0.1$  M Tris concentrations.

Figure 6 provides a comparison in estimated forward rates between 0.1 M Tris solutions at pH = 7, 8, and 9, depicting that pH = 8 and 9 solutions have a direct overlap between Tris-HCl and Tris-HNO<sub>3</sub> rates. However, at pH = 7, a 15-25% reduction in the dissolution rates is observed for Tris-HNO<sub>3</sub> compared to Tris-HCl. Despite this disparity, the high uncertainties displayed in the Tris-HNO<sub>3</sub> rates show near overlap with Tris-HCl fitted rates and their uncertainties ( $\pm 1\sigma$ ; 95% confidence interval), demonstrating close statistical similarities between the estimated rates at pH =

7. Thus, it is deduced that regardless of pH (in the range 7-9), the identity of acid used in Tris-based buffer solutions (i.e. HCl vs. HNO<sub>3</sub>) promotes largely similar glass dissolution behavior.

### 3.3.2.3 Impact of solution pH upon glass dissolution behavior

The impact of the starting pH of Tris-based buffer solutions on the dissolution behavior and kinetics of borosilicate glass is depicted in NL curves in Figures S3(a-c), with the corresponding dissolution rates shown in Figure 6. In each NL curve depicted, the glass exhibits a linear behavior within the first 3-6 h, followed by a transition towards the residual rate regime, where a traditional residual rate behavior has yet to be reached within 24 h for this glass. However, after 24 h of dissolution at pH = 7 and 8 (and 12 h for pH = 9), the NL values for Na and B reach 240-250, 200-210, and 200-220 g/m<sup>2</sup> for pH = 7, 8, and 9, respectively. The estimated forward rate comparisons presented in Figure 6 similarly show that Na dissolution rates remain significantly higher for pH = 7 than pH = 8 and 9, whose rates remain statistically similar. B and Si rates, however, generally show a minimum at pH = 8, where the dissolution rates are higher in pH = 7 and 9 solutions. Previous studies of glass dissolution in varied pH environments (in a wide range of compositions) have suggested that neutral pH exhibits the slowest dissolution rates in comparison to acidic and alkaline media.<sup>16, 23, 56-58</sup> Although our trends suggest minima in dissolution rates to occur at pH = 8 (or between pH = 8 and 9), this shift toward higher pH may occur artificially as a result of solution pH being measured at room temperature (where pH<sub>25 °C</sub> denotes the pH at room temperature), while the local pH at 65 °C is expected to be significantly reduced. For instance, the pH of pure water reduces from 7 (pH<sub>25 °C</sub>) to 6.46 (pH<sub>65 °C</sub>) due to a decrease in pK<sub>w</sub>, attributed to the progression of the forward reaction of H<sub>2</sub>O ⇌ H<sup>+</sup> + OH<sup>-</sup> upon heating and subsequent rise in [H<sup>+</sup>] and [OH<sup>-</sup>].<sup>59</sup> However, the ΔpK<sub>a</sub>/°C value for Tris is -0.031<sup>60</sup> (as compared to ΔpK<sub>w</sub>/°C ≈ -0.026 for pure water<sup>59</sup>), by which it has been calculated using the Henderson-Hasselbalch equation that the pH<sub>65 °C</sub> values of the studied Tris buffer solutions are 5.76, 6.76, and 7.76 for pH<sub>25 °C</sub> = 7, 8, and 9,

respectively, representing a more significant pH reduction at 65 °C than observed for water. The studied solutions are therefore slightly acidic, nearly neutral, and mildly basic at 65 °C (-0.7, +0.3, and +1.3 units compared to neutral for  $\text{pH}_{25\text{ }^\circ\text{C}} = 7, 8, \text{ and } 9$  solutions, respectively). The dissolution rate data displays that  $\text{pH}_{25\text{ }^\circ\text{C}} = 7$  (slightly acidic at 65 °C) solutions exhibit the highest dissolution rates for Na, while  $\text{pH}_{25\text{ }^\circ\text{C}} = 8$  and 9 (slight to moderate alkalinity at 65 °C) solutions exhibit reduced and statistically similar rates. This result indicates that Na release is sensitive to solution acidity ( $[\text{H}^+]/[\text{OH}^-] > 1$  solutions), which is consistent with the established ion exchange mechanism ( $\text{Na}^+ \leftrightarrow \text{H}^+$ ) by which sodium is removed from glasses. B and Si release rates, on the other hand, exhibit minima at  $\text{pH}_{25\text{ }^\circ\text{C}} = 8$ , while solutions lying on either side of this value generally exhibit increased dissolution rates, likely explained by the pH shift with temperature as described in detail above.

### 3.3.3 Evolution of bulk structural characteristics

The glassy grains recovered from dissolution experiments have been analyzed via XRD and MAS NMR spectroscopy. XRD scans of all recovered samples after 12 or 24 hours are completely amorphous, thus ruling out the presence of any crystalline secondary phases (as seen in Figure S4). To quantitatively understand the evolution of glass structure as a function of its dissolution,  $^{11}\text{B}$  MAS NMR spectroscopy has been performed on selected samples subjected to the maximum duration of dissolution in Tris-based solutions (spectra are shown in Figure 7). These spectra have been used to track the structural changes in the borate network, particularly the changes in  $N_4$  fraction in the glass based on integrated areas of  $\text{BO}_3$  and  $\text{BO}_4$  associated peaks (*as has been discussed more in-depth in Section 3.2*). Table 1 presents the  $N_4$  fraction of the glass particles recovered after dissolution for 12-24 h, as compared to that of the as-synthesized glass. The corroded samples exhibit a statistically significant increase in the  $N_4$  fraction (by ~1-3%), considering the  $\pm 0.5\%$   $N_4$  error typically associated with fitting  $^{11}\text{B}$  MAS NMR spectra. These

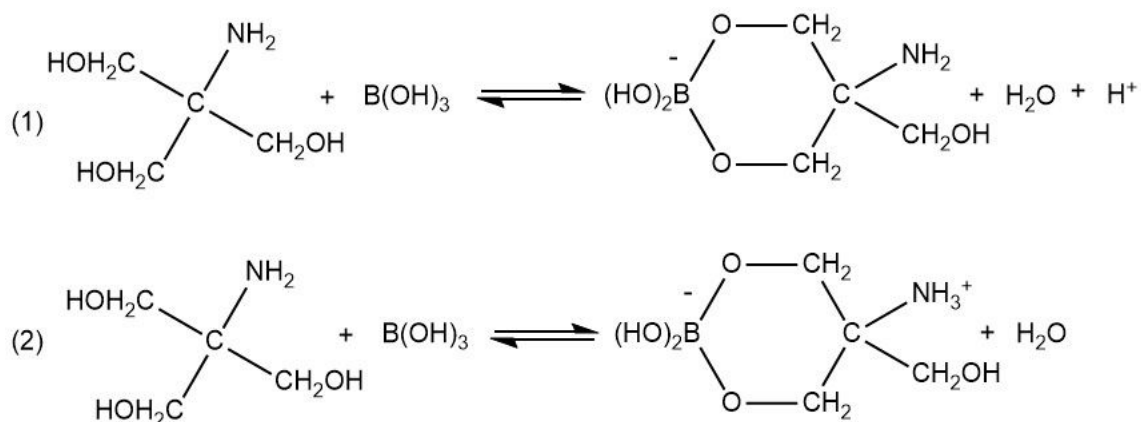
results are consistent with recent literature on aluminoborate, borosilicate, and boroaluminosilicate glass compositions,<sup>61-64</sup> which observe that when the glass comes in contact with water (either from solution or from the atmosphere), an increase in the fraction of tetrahedral B occurs near the glass surface. Generally, in the present study, samples that dissolved at faster rates exhibited larger increases in their  $N_4$  fraction compared to samples exhibiting slower degradation rates. Thus, more reaction progress leads to a larger average B coordination change. For instance, the dissolution of glass in the 0.01 M pH = 8 solutions resulted in nearly 3% increases in  $N_4$ , while in the 0.5 M pH = 8 solutions,  $N_4$  increased by only 1.3%. Further, the B coordination changes are relatively independent of the acid identity used in the Tris buffer solutions. While boron is typically considered as a highly soluble species as evidenced by its use as a tracer element for determining the maximum glass corrosion rate,<sup>12, 65</sup> a few studies have indicated the possibility of boron in hydrated layers in pH = 7-9 conditions.<sup>66-68</sup> Thus, our finding that  $N_4$  increases with the dissolution progress suggests that: (i)  $\text{BO}_3$  units hydrolyze and are released from the glass preferentially in comparison to  $\text{BO}_4$  and/or (ii) amorphous tetrahedral boron units exist near the glass surface as either adsorbed or precipitated species. In either case, less soluble  $\text{BO}_4$  species must exist either within or near the silica gel layers (i.e., a transition region between or across the glass–gel layer interface) or as a part of its own layer on the surface of the gel. However, the precise nature of boron present in hydrated layers requires further structural and compositional examination of the glass–fluid interfacial region.

### *3.3.4 Tracking the identity of aqueous species using liquid NMR*

In an attempt to understand the identity of dissolved boron species as a result of glass dissolution processes (i.e.,  $\text{H}_3\text{BO}_3$  vs. Tris-boron complexes), recovered solution aliquots have been analyzed via  $^{11}\text{B}$  NMR spectroscopy. It should be noted that although the identity of dissolved B species is being probed in the solution environments, these species may initially form either near the

glass surface or merely after boron is released into the surrounding solution. In the present study, the NMR experiments have been performed at both room temperature and at 65 °C. The latter temperature has been selected to reproduce the experimental dissolution conditions in order to understand the impact of temperature on the nature of the dissolved species resulting from glass dissolution processes.

Figure 8a displays  $^{11}\text{B}$  NMR spectra of selected solutions at 25 °C, which have been compared to the reference solution as has been described in *section 2.4.2*. This reference solution mixture, which comprises a Tris/B = 1 ratio, displays peaks in two main regions, (i) an intense sharp peak associated with  $\text{H}_3\text{BO}_3$  (near 19.0 ppm) and (ii) two additional sharp peaks in the range 0.6-1.2 ppm. The upfield peaks observed in our reference medium notably show consistency with an identical solution mixture (pH = 7.5) in the study by Tournié et al.<sup>25</sup>, thus, are attributed to Tris-boron complexes. Following the identification of these complexes in Ref.<sup>25</sup>, we attribute the two distinct peaks near 0.6 and 1.2 ppm to Tris-borate and Tris-boric complexes, respectively, which form in solution according to the following reactions:<sup>25</sup>



where reaction (1) depicts Tris-borate formation and reaction (2) depicts Tris-boric formation. The upfield chemical shift of the Tris-boric complex compared to Tris-borate arises from the extra hydrogen on its amine group, similar to as previously observed for protonated amines in  $^{13}\text{C}$  chemical shifts.<sup>69</sup> Consistent with the above molecular structures, the observed shift values of 19.0

and 0.6-1.2 ppm in the studied  $^{11}\text{B}$  spectra are typical of 3- and 4-coordinated boron species,<sup>45</sup> respectively, where the former indicates aqueous  $\text{H}_3\text{BO}_3$  and the latter indicate Tris-boron complexes existing in four-fold coordination. It should be noted that the peaks observed in our reference sample do not show direct chemical shift alignment with those in the previous study ( $\sim 22$  and  $\sim 4$  ppm, respectively<sup>25</sup>), however, we believe that this discrepancy arises as a result of a chemical shift referencing error by Tournié et al.,<sup>25</sup> since each peak is shifted  $\sim 3$  ppm downfield from the presently observed resonances. Furthermore, our measured shift for aqueous  $\text{H}_3\text{BO}_3$  is consistent with the value of 19.6 ppm reported in the literature.<sup>70</sup>

The  $^{11}\text{B}$  NMR spectra of solutions recovered from selected dissolution experiments are also pictured in Figure 8a. These solutions, interestingly, consist of either one or two sharp peaks at 0.5-0.6 and 1.1-1.2 ppm of varying intensities (typical of Tris-borate and Tris-boric complexes, respectively) and are marked by the absence of clear  $\text{H}_3\text{BO}_3$  peaks (except for 0.1 M Tris- $\text{HNO}_3$  at  $\text{pH} = 7$ ). This finding signifies that, at room temperature, dissolved boron from the glass exists predominantly as Tris-boron complexes as opposed to boric acid species. Further, it is observed at  $\text{pH} = 8$  that the intensity of Tris-borate and Tris-boric peaks varies remarkably with Tris molarity in the solution. For instance, the 0.01 M Tris- $\text{HNO}_3$  solution portrays a peak associated with Tris-borate complexes. However, an increase in Tris molarity leads to the development of a Tris-boric complex peak which dominates the  $^{11}\text{B}$  NMR signal in the 0.5 M Tris- $\text{HNO}_3$  solution.

Figure 8b, on the other hand, depicts  $^{11}\text{B}$  NMR spectra of the same solutions at 65 °C. These spectra have also been compared to the same Tris/B = 1 reference mixture as described above. At 65 °C, the spectra of the reference mixture at  $\text{pH} = 8$  displays only a peak associated with  $\text{H}_3\text{BO}_3$  centered near 19.7 ppm, while the peaks associated with Tris-boron complexes are absent. Similarly, the spectra of liquid aliquots recovered from 24 h of dissolution experiments (examined at 65 °C) also lack Tris-boron complex peaks in the range of 0.5-1.2 ppm, rather displaying only

one peak associated with  $\text{H}_3\text{BO}_3$  species (in the range 19.4-19.8 ppm). This crucial difference between  $^{11}\text{B}$  NMR spectra acquired at room temperature and 65 °C implies that, while Tris-boron complexes are stable and form spontaneously at room temperature, increasing the surrounding temperature causes reactions (1) and (2) to move towards the left and revert to unassociated boric acid species and Tris molecules in solution. Further, this finding indicates that the forward reaction is exothermic and can be reversed upon addition of sufficient heat to the system.

The absence of peaks associated with Tris-boron complexes from both experimentally recovered solutions and prepared Tris/B mixtures at 65 °C is particularly intriguing since this temperature coincides with the experimental dissolution conditions. This suggests that, in the experimental conditions used in the present study, zero or negligible concentrations of Tris-boron complexes are present in solution, even in samples with higher reaction progress (i.e., liquids recovered from the dissolution experiments approaching the residual rate regime). Thus, even though the presence of Tris-boron complexes has been determined to be extensive at room temperature, their absence in higher temperature conditions indicates that the formation of Tris-boron complexes may not serve as the primary mechanism governing the dissolution behavior of borosilicate glasses in Tris-based solutions at elevated temperatures. However, this hypothesis requires further investigation using *in situ* NMR spectroscopy to track and identify dissolved species characteristics during dissolution at high temperatures.

It should also be noted here that only the spectra from certain Tris-based solutions at 65 °C are shown in Figure 8b since these spectra contained readily detectable  $^{11}\text{B}$  NMR signals. Attempts were also made to acquire the  $^{11}\text{B}$  NMR spectra from the post-dissolution liquid aliquots of Tris-HCl and Tris- $\text{HNO}_3$  solutions with 0.1 M Tris (pH = 8 and 9) and 0.5 M Tris (pH = 8). However, the concentration of aqueous  $^{11}\text{B}$  nuclei in these samples was apparently at or below detection limits necessary to resolve and identify dissolved boron species. Therefore, at present, we cannot

comment on the dissolved species removed from glass submerged in these solutions at elevated temperatures.

### 3.3.5 Surface chemistry of dissolved bulk coupons

Additional dissolution experiments were performed on polished glass coupons to analyze the chemical composition of the alteration layers forming on the glass surface, as a result of the dissolution processes. The studied glass samples were subjected to 24 hours of submersion in 0.1 M Tris-HCl or Tris-HNO<sub>3</sub> at pH = 7 and analyzed using XPS and ERDA for their surface composition and comparison to the polished (and uncorroded) glass surface. Table 2 provides surface elemental compositions of the glass coupons as determined from XPS. It is observed that the comparison between the bulk composition and the polished surface is close for all the elements present in the sample, i.e., Na ( $\pm 1\%$ ), B ( $\pm 5\%$ ), Si ( $\pm 1\%$ ), and O ( $\pm 4\%$ ). Following 24 h of dissolution in pH = 7 solutions, the surfaces of the glass coupons (top  $\sim 3$ -10 nm) were completely devoid of boron, while sodium content was reduced by at least 90%, as shown in Figures 9a and 9b, respectively. Si and O, on the other hand, are significantly enriched at the surface and exist as the primary components, shown in Figures 9c and 9d, respectively, with an O/Si ratio of  $\sim 2.8$ -2.9 (representing a higher O/Si than the stoichiometry of pure silica). The shift towards higher binding energy as observed in Si 2p and O 1s spectra is consistent with literature of similar borosilicate glass compositions and of silica gel layers.<sup>71-73</sup> Accordingly, the immediate surface layers closest to the glass–fluid interface likely consist of a silicate network depolymerized by hydroxyl groups, as confirmed from ERDA studies (discussed below). Further, the absence of boron species in these layers is intriguing, given the results from <sup>11</sup>B MAS NMR studies indicating the potential presence of B within the silica gel layer. However, it is important to note that equivalent thickness calculations (made by dividing the term  $N_{\text{B or Na}} - N_{\text{Si}}$  by the glass density)<sup>67</sup> estimate that the thickness of the dissolved layer after 24 h in the studied conditions is  $\sim 50$ -60  $\mu\text{m}$ , while the present XPS analysis probes at maximum only  $\sim 10$

nm into the glass surface. Thus, it is likely that if boron species are present in the interfacial layers, they exist in subsurface regions closer to the reactive interface between pristine glass and gel.

The ERDA spectra of the uncorroded and corroded glass coupons are displayed in Figure 10. As expected, it is evident from these spectra, which probe approximately the top ~350 nm of the glass surface, that the dissolved samples contain a significant signal from hydrogen on the surface as compared to the polished, uncorroded analog. These results verify that a silica gel layer exists on the glass surface, which is also corroborated from FTIR data (FTIR-UATR; as described in *section 2.4.1*) on powder samples (see Figure S5), displaying an absorption band at 1220  $\text{cm}^{-1}$  characteristic of Si-OH bonding<sup>74</sup> as well as multiple bands in the region 3000-3700  $\text{cm}^{-1}$  associated with various O-H stretching vibrations of free/bonded water and silanol units near the glass surface.<sup>75</sup> The ERDA spectra were fitted to quantify the atomic hydrogen content in this layer, which are listed in Table 2. Slight differences in H content are observed with acid identity (within  $\pm 2\%$ ), indicating slight differences in the content of hydroxyl groups and/or water confined within the gel layer. However, significant differences in gel layer characteristics are not expected given the similarity in elemental release displayed regardless of the acid identity.

#### 4. Discussion

It is generally agreed in the glass community that the addition of additives such as buffering agents, chelators, or salt/salinity represents a risk to modifying the apparent release rates of glass in corroding solutions, with Tris-based buffer solutions being no exception. Here, the dissolution of boron-containing glasses in Tris solutions has come under particular questioning due to the evidence of Tris-boron complexation, which is hypothesized to accelerate the release of dissolution products from the sample surface. However, much of this view can be attributed to a single study that observed (i) Tris-boron complexes in 1:1 Tris/B solution mixtures and (ii) significant forward rate acceleration of a sodium borosilicate glass in Tris-based solutions vs. Tris-free solutions.<sup>25</sup> That

said, many aspects of Tris–glass interactions are still uncertain, for instance, how does the concentration of Tris at fixed buffer pH impact the dissolution behavior of a glass? And does the identity of the strong acid counter-ion play a role in the apparent dissolution kinetics of a glass?

The present study aims to address these questions by investigating the dissolution behavior of a sodium borosilicate composition in a range of aqueous environments, in which the impacts of acid identity, Tris molarity, and solution pH are examined. Contrary to the findings by Tournié et al.,<sup>25</sup> which displayed 2× quicker elemental release in Tris-HCl as compared to Tris-HNO<sub>3</sub>, the present contribution does not illustrate significant differences in the dissolution behavior based on acid identity. This is evidenced by the close overlap in the elemental release behavior between 0.1 M Tris-HCl and 0.1 M Tris-HNO<sub>3</sub> solutions, as displayed at pH = 7-9 in Figures 6 and S3. Furthermore, all estimated forward rates (Tris-HCl vs. Tris-HNO<sub>3</sub>) display close agreement, well within the generally accepted error limits while assessing the dissolution behavior.<sup>51, 54, 55</sup> Thus, our findings indicate that acid identity does not greatly impact borosilicate dissolution behavior in Tris buffer solutions.

Further, the glass' dissolution kinetics has been investigated at pH = 8 in Tris molarities varying from 0.01 – 0.5 M. As anticipated, higher Tris molarities are more effective in buffering the solution pH, as  $\geq 0.1$  M Tris-based solutions maintained pH within  $\pm 0.1$  after 24 h of dissolution experiments. Conversely, it is observed that increasing the Tris molarity from 0.01 to 0.5 M results in the suppression of the elemental release from glass, as is particularly evident from the contrast between 0.01-0.1 M Tris solutions and 0.3-0.5 M solutions (see Figure 5). It is inferred from these results that the substantial presence of the dissolved species in 0.3 and 0.5 M solutions provokes solution feedback effects, thus, suppressing the extent of glass dissolution. According to these results, it is deduced that an ideal Tris concentration is required to provide a balance between (i) optimal buffering capacity to stabilize solution pH and avoid its evolution over the course of the

experiment, while (ii) minimally impacting the dissolution kinetics—at the very least within the forward rate regime. In these experiments, this concentration is  $\sim 0.1$  M Tris, independent of acid identity (Tris-HCl vs. Tris-HNO<sub>3</sub>). This value corresponds closely with the recommended Tris concentrations as discussed in ISO standards 10993-14 and 23317 for studying biomaterials in simulated body environments, in addition to previous literature discussing corrosion of glasses for nuclear waste containment or of geological importance.<sup>4-6, 9, 12, 18, 20</sup> Notably, for other glasses of markedly differing composition, the buffering capacity needs of the experiment will be dictated by the ion release rate(s) of that glass' particular constituents; for example, with a glass with a very high concentration of alkali and rapid release rates, 0.1 M Tris concentration may not sufficiently stabilize pH over the experimental timeframe.

Further, in accordance with the findings by Tournié et al.,<sup>25</sup> the presence of Tris-boron complexes has been confirmed in the examined solution aliquots. Interestingly, the two identified complexes are observed to demonstrate clear temperature-dependence, marked by their spontaneous formation in aliquots at room temperature (Reactions (1) and (2)) and complete absence of the same complexes in the aliquots at 65 °C. Rather, applying heat to NMR experiments promotes the reverse reactions of (1) and (2), causing instability of Tris-boron complexes and conversion to boric acid species and Tris molecules. This unanticipated temperature-dependence of Tris-boron complexation requires further examination using *in situ* NMR spectroscopy to examine the mechanisms by which Tris-based solutions impact borosilicate glass dissolution behavior and kinetics.

## 5. Conclusions

In the present study, a sodium borosilicate glass has been examined for its dissolution behavior in a wide range of Tris-based solutions. The results have been discussed with reference to previous studies on this topic and the conclusions from this study are threefold: (i) acid identity does not greatly impact the dissolution behavior in Tris-based solutions, (ii)  $\sim 0.1$  M Tris-based

solutions are ideal for sustaining solution pH in the absence of clear adverse solution chemistry effects, and (iii) Tris-boron complexes form as a result of glass dissolution processes. However, complex formation exhibits a clear temperature-dependence and requires further study to unearth the mechanisms by which Tris-based solutions impact the dissolution behavior of borosilicate glasses.

### **Conflicts of interest**

The authors confirm the absence of any conflict of interest with this submission.

### **Acknowledgments**

This material is based upon work supported by the National Science Foundation under Grant No. 1507131 and 2034871, and the US Department of Energy, Offices of Nuclear Energy and Environmental Management through Nuclear Energy University Program (Contract No. DE-NE0008597). ORNL is operated by UT-Battelle, LLC for the US DOE under Contract No.'s DE-AC05-00OR22725. The authors also thank the Characterization Sciences group at Corning Incorporated for the compositional analysis of the glass.

## References

1. International Organization for Standardization, ISO 10993-14: *Biological evaluation of medical devices – Part 14: Identification and quantification of degradation products from ceramics*, International organization for standardization technical report, 2001.
2. International Organization for Standardization, ISO 23317: *Implants for surgery – In vitro evaluation for apatite-forming ability of implant materials*, International organization for standardization technical report, 2014.
3. ASTM (American Society for Testing and Materials) Standard: C1220-17, *ASTM International*, West Conshohocken, PA, 2017.
4. E. M. Pierce, L. R. Reed, W. J. Shaw, B. P. McGrail, J. P. Icenhower, C. F. Windisch, E. A. Cordova and J. Broady, *Geochim. Cosmochim. Acta*, 2010, **74**, 2634-2654.
5. E. M. Pierce, E. A. Rodriguez, L. J. Calligan, W. J. Shaw and B. P. McGrail, *Appl. Geochem.*, 2008, **23**, 2559-2573.
6. J. P. Icenhower, B. P. McGrail, W. J. Shaw, E. M. Pierce, P. Nachimuthu, D. K. Shuh, E. A. Rodriguez and J. L. Steele, *Geochim. Cosmochim. Acta*, 2008, **72**, 2767-2788.
7. M. Kinoshita, M. Harada, Y. Sato and Y. Hariguchi, *J. Am. Ceram. Soc.*, 1991, **74**, 783-787.
8. T. C. Kaspar, J. T. Reiser, J. V. Ryan and N. A. Wall, *J. Non-Cryst. Solids*, 2018, **481**, 260-266.
9. D. J. Backhouse, A. J. Fisher, J. J. Neeway, C. L. Corkhill, N. C. Hyatt and R. J. Hand, *npj Materials Degradation*, 2018, **2**, 1-10.
10. E. M. Pierce, E. L. Richards, A. M. Davis, L. R. Reed and E. Rodriguez, *Environ. Chem.*, 2008, **5**, 73-85.
11. D. J. Wesolowski and D. A. Palmer, *Geochim. Cosmochim. Acta*, 1994, **58**, 2947-2969.
12. N. Rajmohan, P. Frugier and S. Gin, *Chem. Geol.*, 2010, **279**, 106-119.
13. P. Frugier, Y. Minet, N. Rajmohan, N. Godon and S. Gin, *npj Materials Degradation*, 2018, **2**, 1-13.
14. A. Ledieu, F. Devreux, P. Barboux, L. Sicard and O. Spalla, *J. Non-Cryst. Solids*, 2004, **343**, 3-12.
15. F. Angeli, D. Boscarino, S. Gin, G. D. Mea, B. Boizot and J. Petit, *Phys. Chem. Glasses*, 2001, **42**, 279-286.
16. G. Perera and R. H. Doremus, *J. Am. Ceram. Soc.*, 1991, **74**, 1554-1558.
17. P. Jollivet, L. Galoisy, G. Calas, F. Angeli, S. Gin, M. Ruffoni and N. Trcera, *J. Non-Cryst. Solids*, 2019, **503**, 268-278.
18. J. J. Neeway, P. C. Rieke, B. P. Parruzot, J. V. Ryan and R. M. Asmussen, *Geochim. Cosmochim. Acta*, 2018, **226**, 132-148.
19. M. Arab, C. Cailleateau, F. Angeli, F. Devreux, L. Girard and O. Spalla, *J. Non-Cryst. Solids*, 2008, **354**, 155-161.
20. J. Hopf, S. N. Kerisit, F. Angeli, T. Charpentier, J. P. Icenhower, B. P. McGrail, C. F. Windisch, S. D. Burton and E. M. Pierce, *Geochim. Cosmochim. Acta*, 2016, **181**, 54-71.
21. G. Gomori, *Proc. Soc. Exp. Biol. Med.*, 1946, **62**, 33-34.
22. W. L. Ebert, *The effects of the glass surface area/solution volume ratio on glass corrosion: a critical review*, Argonne National Laboratory, 1995.
23. B. C. Bunker, *J. Non-Cryst. Solids*, 1994, **179**, 300-308.
24. P. Jollivet, S. Gin and S. Schumacher, *Chem. Geol.*, 2012, **330-331**, 207-217.
25. A. Tournié, O. Majérus, G. Lefèvre, M. N. Rager, S. Walmé, D. Caurant and P. Barboux, *J. Colloid Interface Sci.*, 2013, **400**, 161-167.
26. J. Hlavac, D. Rohanova and A. Helebrant, *Ceram.–Silik.*, 1994, **38**, 119-119.
27. D. Rohanová, A. R. Boccaccini, D. M. Yunos, D. Horkavcová, I. Březovská and A. Helebrant, *Acta Biomater.*, 2011, **7**, 2623-2630.
28. D. Rohanová, D. Horkavcova, L. Paidere, A. R. Boccaccini, P. Bozděchová and P. Bezdička, *J. Biomed. Mater. Res. B*, 2018, **106**, 143-152.
29. D. Horkavcová, D. Rohanová, A. Stříbny, K. Schuhladden, A. R. Boccaccini and P. Bezdička, *J. Biomed. Mater. Res. B*, 2020, **108**, 1888-1896.

30. G. Kirste, J. Brandt-Slowik, C. Bocker, M. Steinert, R. Geiss and D. S. Brauer, *Int. J. Appl. Glass Sci.*, 2017, **8**, 438-449.
31. T. Steenberg, H. K. Hjenner, S. L. Jensen, M. Guldborg and T. Knudsen, *Glastech. Ber. Glass Sci. Technol.*, 2001, **74**, 97-105.
32. A. Violante and P. Violante, *Clays Clay Miner.*, 1980, **28**, 425-434.
33. L. Björkvik, X. Wang and L. Hupa, *Int. J. Appl. Glass Sci.*, 2016, **7**, 154-163.
34. D. J. Wesolowski, D. A. Palmer and G. M. Begun, *J. Solution Chem.*, 1990, **19**, 159-173.
35. N. Stone-Weiss, E. M. Pierce, R. E. Youngman, O. Gulbiten, N. J. Smith, J. Du and A. Goel, *Acta Biomater.*, 2018, **65**, 436-449.
36. S. Gin, A. Abdelouas, L. J. Criscenti, W. L. Ebert, K. Ferrand, T. Geisler, M. T. Harrison, Y. Inagaki, S. Mitsui and K. T. Mueller, *Mater. Today*, 2013, **16**, 243-248.
37. P. Balasubramanian, T. Buettner, V. M. Pacheco and A. R. Boccaccini, *J. Eur. Ceram. Soc.*, 2018, **38**, 855-869.
38. A. Hoppe, N. S. Gueldal and A. R. Boccaccini, *Biomaterials*, 2011, **32**, 2757-2774.
39. O. Mazurin, M. Streltsina and T. Shvaiko-Shvaikovskaya, *Institute of Theoretical Chemistry, Shrewsbury, MA, USA*, 2005.
40. D. Massiot, F. Fayon, M. Capron, I. King, S. Le Calvé, B. Alonso, J. O. Durand, B. Bujoli, Z. Gan and G. Hoatson, *Magn. Reson. Chem.*, 2002, **40**, 70-76.
41. D. Massiot, C. Bessada, J. Coutures and F. Taulelle, *J. Magn. Reson.*, 1990, **90**, 231-242.
42. J. H. Scofield, *Theoretical photoionization cross sections from 1 to 1500 keV*, California Univ., Livermore. Lawrence Livermore Lab., 1973.
43. G. C. Smith, *J. Electron. Spectrosc.*, 2005, **148**, 21-28.
44. S.A. Feller, J. Kottke, J. Welter, S. Nijhawan, R. Boekenhauer, H. Zhang, D. Feil, C. Parameswar, K. Budhwani, M. Affatigato, A. Bhatnagar, G. Bhasin, S. Bhowmik, J. Mackenzie, M. Royle, M. Kambeyanda, P. Pandikuthira, M. Sharma, *Proceedings of the Second International Conference on Borate Glasses, Crystals, and Melts, The Society of Glass Technology, Sheffield, UK*, 1997, 223-230.
45. L.-S. Du and J. F. Stebbins, *J. Phys. Chem. B*, 2003, **107**, 10063-10076.
46. Y. H. Yun and P. J. Bray, *J. Non-Cryst. Solids*, 1978, **27**, 363-380.
47. W. J. Dell, P. J. Bray and S. Z. Xiao, *J. Non-Cryst. Solids*, 1983, **58**, 1-16.
48. P. J. Bray, *J. Non-Cryst. Solids*, 1985, **75**, 29-36.
49. J. Hopf, J. R. Eskelsen, M. Chiu, A. Ievlev, O. S. Ovchinnikova, D. Leonard and E. M. Pierce, *Geochim. Cosmochim. Acta*, 2018, **229**, 65-84.
50. J. D. Vienna, J. V. Ryan, S. Gin and Y. Inagaki, *Int. J. Appl. Glass Sci.*, 2013, **4**, 283-294.
51. W. L. Ebert, *Comparison of the results of short-term static tests and single-pass flow-through tests with LRM glass (ANL-06/51)*, Argonne National Laboratory (ANL), 2007.
52. J. Kragten, *Analyst*, 1994, **119**, 2161-2165.
53. N. Stone-Weiss, R. E. Youngman, R. Thorpe, N. J. Smith, E. M. Pierce and A. Goel, *Phys. Chem. Chem. Phys.*, 2020, **22**, 1881-1896.
54. S. Gin, P. Frugier, P. Jollivet, F. Bruguier and E. Curti, *Int. J. Appl. Glass Sci.*, 2013, **4**, 371-382.
55. M. Fournier, A. Ull, E. Nicoleau, Y. Inagaki, M. Odorico, P. Frugier and S. Gin, *J. Nucl. Mater.*, 2016, **476**, 140-154.
56. J. P. Hamilton, S. L. Brantley, C. G. Pantano, L. J. Criscenti and J. D. Kubicki, *Geochim. Cosmochim. Acta*, 2001, **65**, 3683-3702.
57. D. Wolff-Boenisch, S. R. Gislason, E. H. Oelkers and C. V. Putnis, *Geochim. Cosmochim. Acta*, 2004, **68**, 4843-4858.
58. Y. Inagaki, T. Kikunaga, K. Idemitsu and T. Arima, *Int. J. Appl. Glass Sci.*, 2013, **4**, 317-327.
59. A. V. Bandura and S. N. Lvov, *J. Phys. Chem. Ref. Data*, 2006, **35**, 15-30.
60. N. E. Good, G. D. Winget, W. Winter, T. N. Connolly, S. Izawa and R. M. Singh, *Biochemistry*, 1966, **5**, 467-477.
61. S. Kapoor, R. E. Youngman, K. Zakharchuk, A. Yaremchenko, N. J. Smith and A. Goel, *J. Phys. Chem. B*, 2018, **122**, 10913-10927.

62. R. A. Schaut, R. A. Lobello, K. T. Mueller and C. G. Pantano, *J. Non-Cryst. Solids*, 2011, **357**, 3416-3423.
63. N. J. Smith, C. V. Cushman, M. R. Linford, R. A. Schaut, J. Banerjee, R. E. Youngman, L. Thomsen, L. S. Fisher, A. J. Barlow and P. J. Pigram, *J. Non-Cryst. Solids*, 2020, **545**, 120247.
64. S. H. Garofalini, M. T. Ha and J. Urraca, *J. Am. Ceram. Soc.*, 2018, **101**, 1135-1148.
65. B. E. Scheetz, W. P. Freeborn, D. K. Smith, C. Anderson, M. Zolensky and W. B. White, *Mater. Res. Soc. Symp. Proc.*, 1985, **44**, 129-134.
66. S. Gin, L. Neill, M. Fournier, P. Frugier, T. Ducasse, M. Tribet, A. Abdelouas, B. Parruzot, J. Neeway and N. Wall, *Chem. Geol.*, 2016, **440**, 115-123.
67. S. Gin, P. Jollivet, M. Fournier, C. Berthon, Z. Wang, A. Mitroshkov, Z. Zhu and J. V. Ryan, *Geochim. Cosmochim. Acta*, 2015, **151**, 68-85.
68. S. Gin, P. Jollivet, M. Fournier, F. Angeli, P. Frugier and T. Charpentier, *Nat. Commun.*, 2015, **6**, 6360.
69. E. J. Sudhölter, R. Huis, G. R. Hays and N. C. Alma, *J. Colloid Interface Sci.*, 1985, **103**, 554-560.
70. M. J. Dewar and R. Jones, *J. Am. Chem. Soc.*, 1967, **89**, 2408-2410.
71. J. F. Moulder, W. Stickle, P. Sobol and K. Bomben, *Inc., Japan*, 1995.
72. Y. Miura, H. Kusano, T. Nanba and S. Matsumoto, *J. Non-Cryst. Solids*, 2001, **290**, 1-14.
73. T. Gross, M. Ramm, H. Sonntag, W. Unger, H. Weijers and E. Adem, *Surf. Interface Anal.*, 1992, **18**, 59-64.
74. A. Goel, S. Kapoor, A. Tilocca, R. R. Rajagopal and J. M. F. Ferreira, *J. Mater. Chem. B*, 2013, **1**, 3073-3082.
75. D. Rébiscoul, F. Bruguier, V. Magnin and S. Gin, *J. Non-Cryst. Solids*, 2012, **358**, 2951-2960.

## Figure Captions

**Figure 1.** The  $^{11}\text{B}$  MAS NMR spectrum and the fitted lineshape for the as-synthesized glass. This spectrum was fitted with two Q mas  $\frac{1}{2}$  components for the B(III) resonances and three Gauss/Lorentz functions for the B(IV) resonances. The minor fitted peak displayed near 0 ppm represents the central peak of the satellite transition manifold of the B(IV) resonance, which overlaps with the MAS peak of the central transition, and whose area needs to be considered when extracting the  $N_4$  value from the spectrum.

**Figure 2.** pH vs. time for all studied Tris-HCl and Tris-HNO<sub>3</sub> solutions, organized according to starting pH and Tris molarity.

**Figure 3.** NL vs. time curves for the studied glass in (a) pH = 7, (b) pH = 8, and (c) pH = 9 Tris-HNO<sub>3</sub> solutions.

**Figure 4.** NL vs. time for B in (a) Tris-HCl and (b) Tris-HNO<sub>3</sub> solutions at pH = 8. Each plot displays the NL curve differences in Tris solution molarities ranging from 0.01 – 0.5 M.

**Figure 5.** Dissolution rate vs. Tris molarity in solution for all elements in pH = 8 Tris-HCl and Tris-HNO<sub>3</sub> solutions.

**Figure 6.** Dissolution rate vs. starting solution pH for all elements in 0.1 M Tris-HCl and Tris-HNO<sub>3</sub> solutions at pH = 7, 8, and 9.

**Figure 7.**  $^{11}\text{B}$  MAS NMR spectra of powders recovered from 24 h of selected experiments. (\*) Denotes that the powders were recovered from 12 h experiments.

**Figure 8.**  $^{11}\text{B}$  liquid NMR spectra of liquid aliquots recovered from 24 h of dissolution experiments. (\*) Denotes that the solutions were recovered from 12 h experiments.

**Figure 9.** (a) B 1s, (b) Na 1s, (c) Si 2p, and (d) O 1s XPS spectra of polished and dissolved glass coupons (24 hours in 0.1 M Tris-HCl and Tris-HCl solutions at pH = 7).

**Figure 10.** ERDA spectra of the polished (un-corroded) monolithic glass sample, compared to monolithic glass samples dissolved for 24 h in 0.1 M Tris buffer solutions (pH = 7).

## Figures

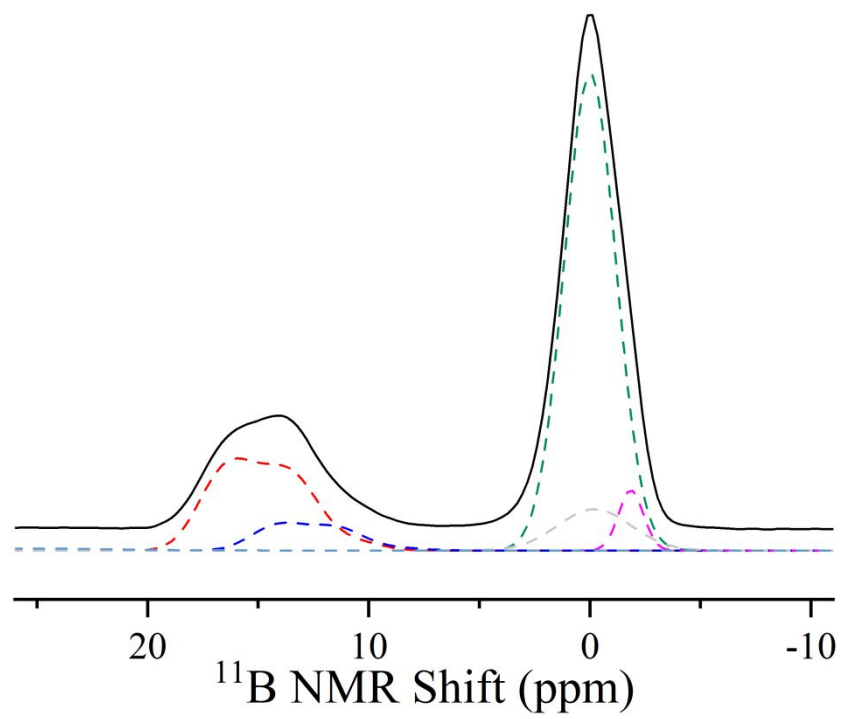


Figure 1

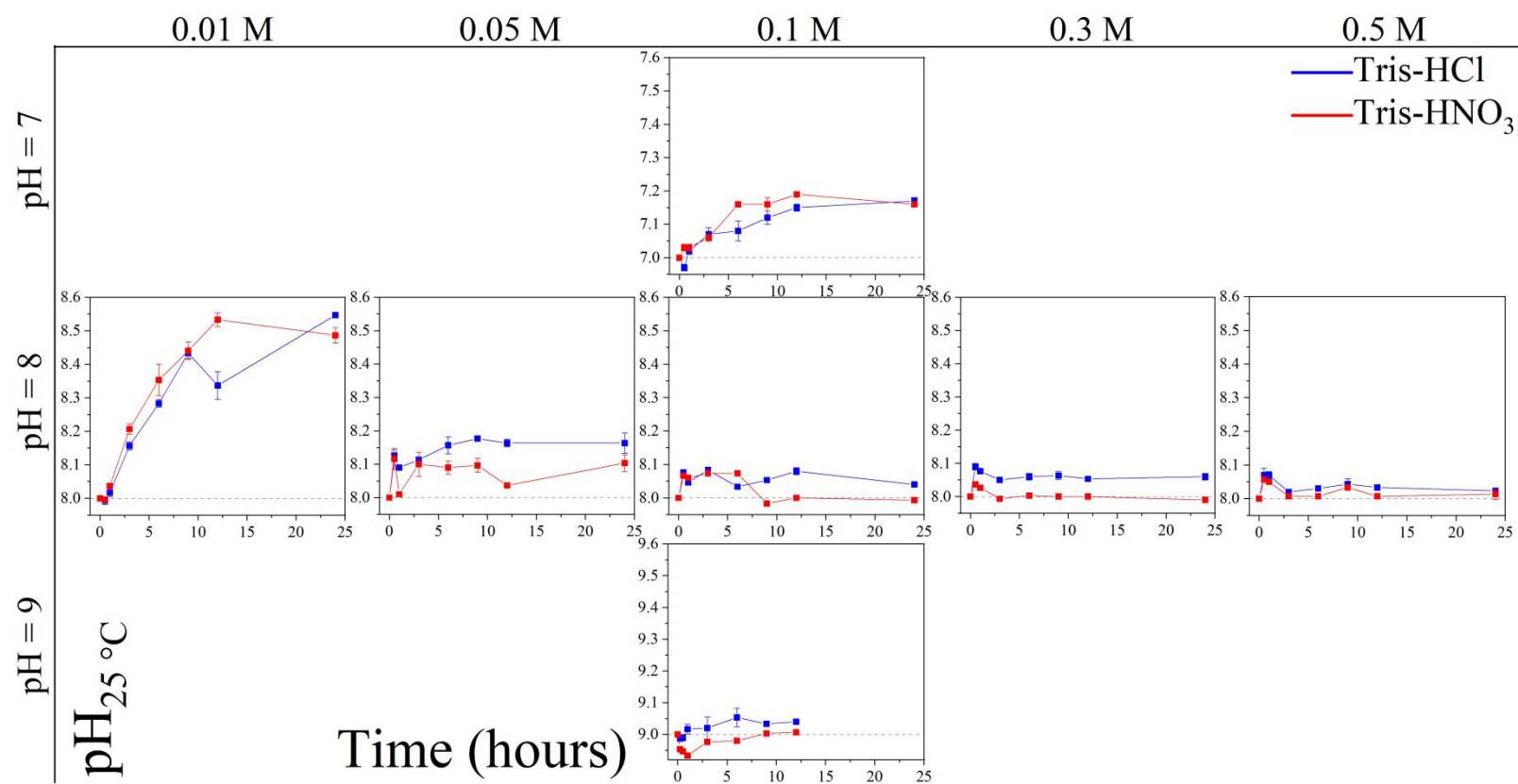


Figure 2

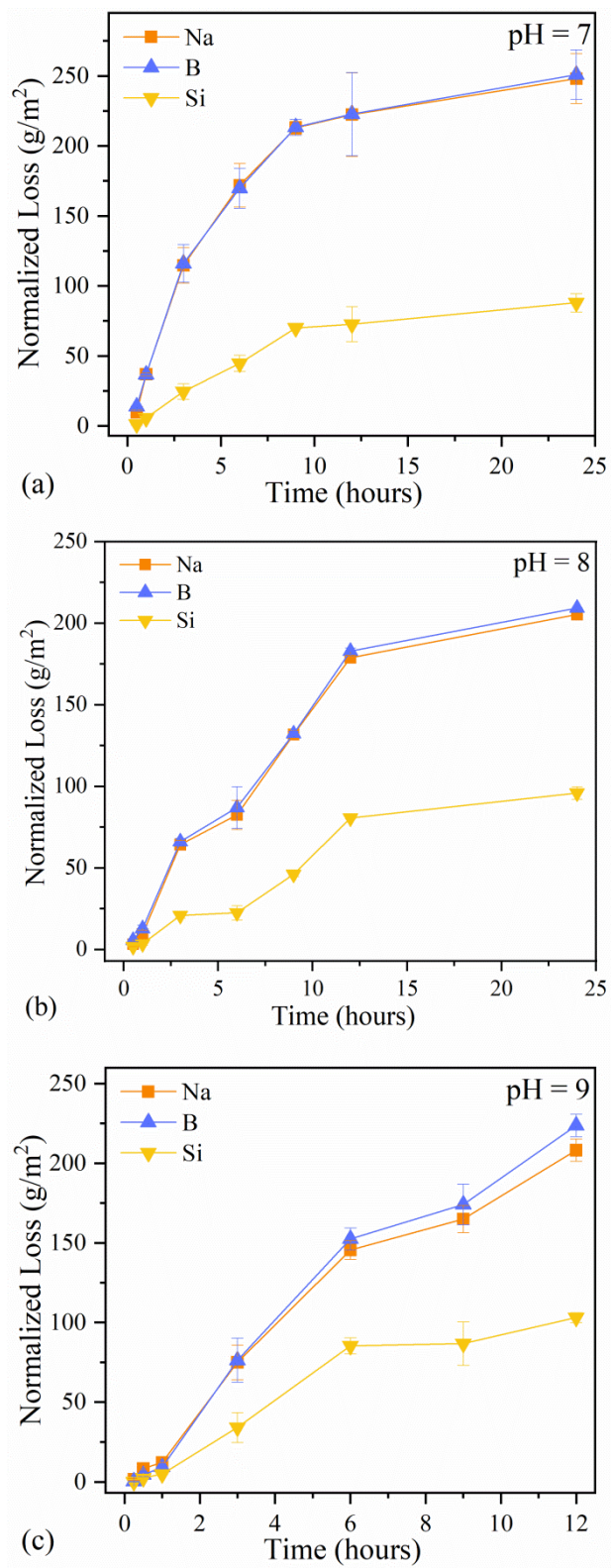


Figure 3

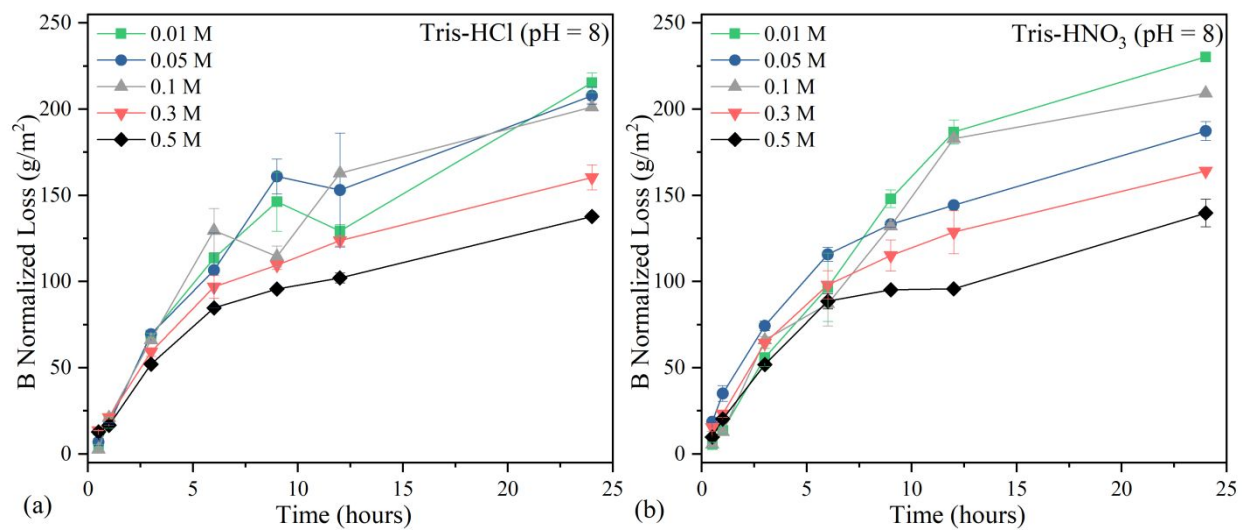


Figure 4

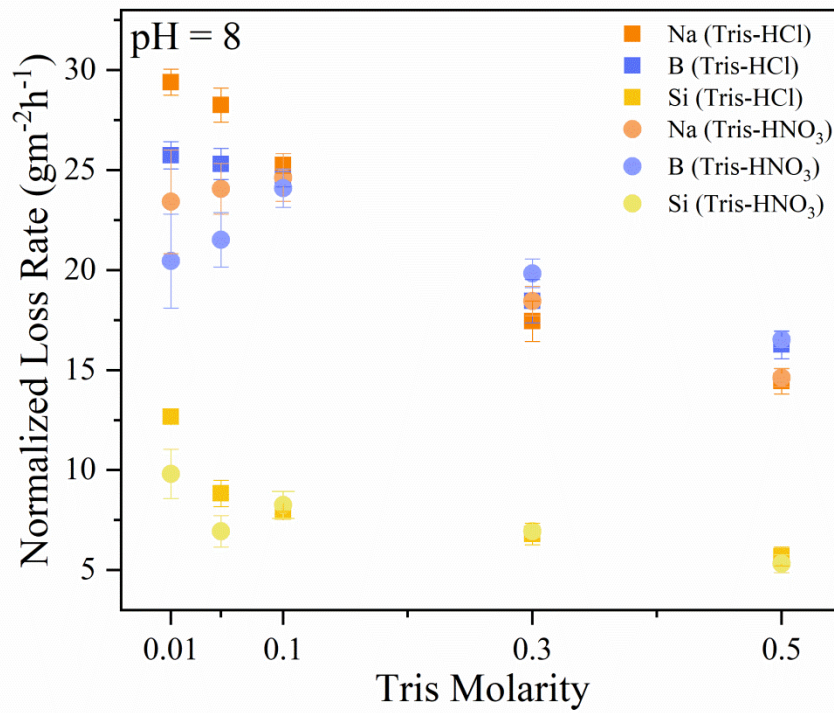


Figure 5

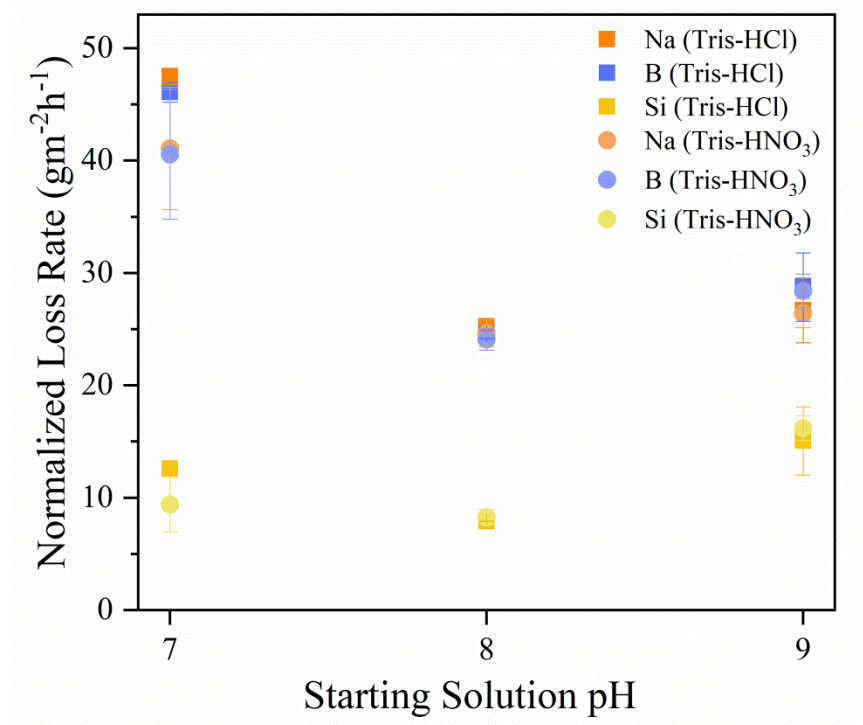


Figure 6

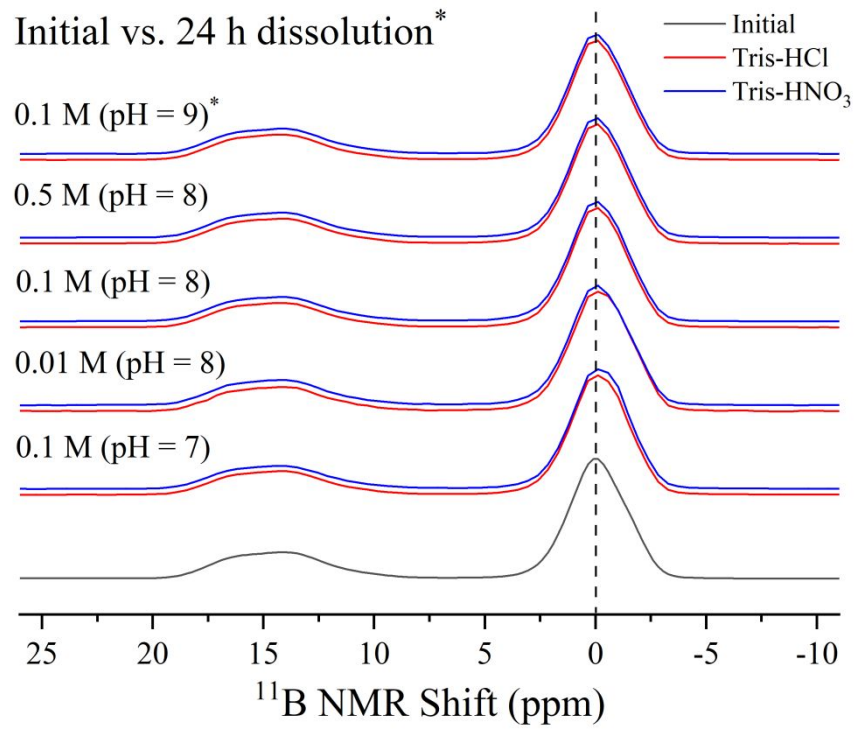


Figure 7

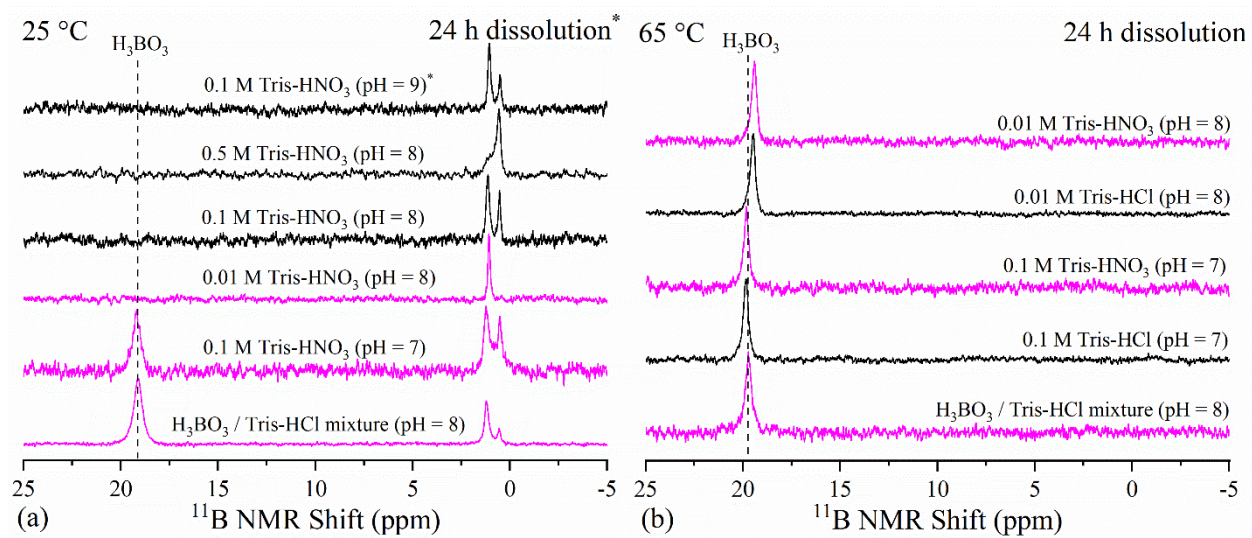


Figure 8

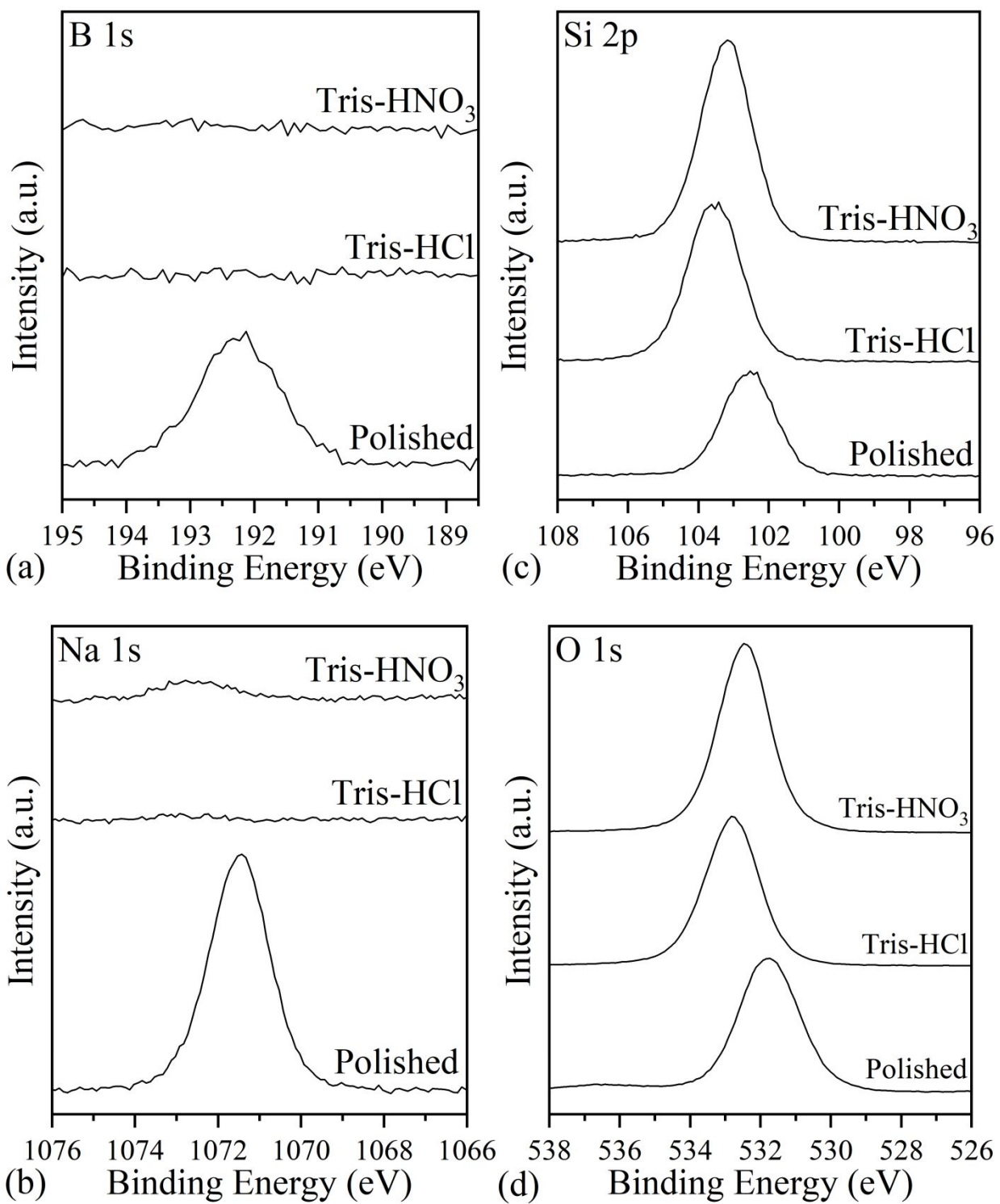


Figure 9

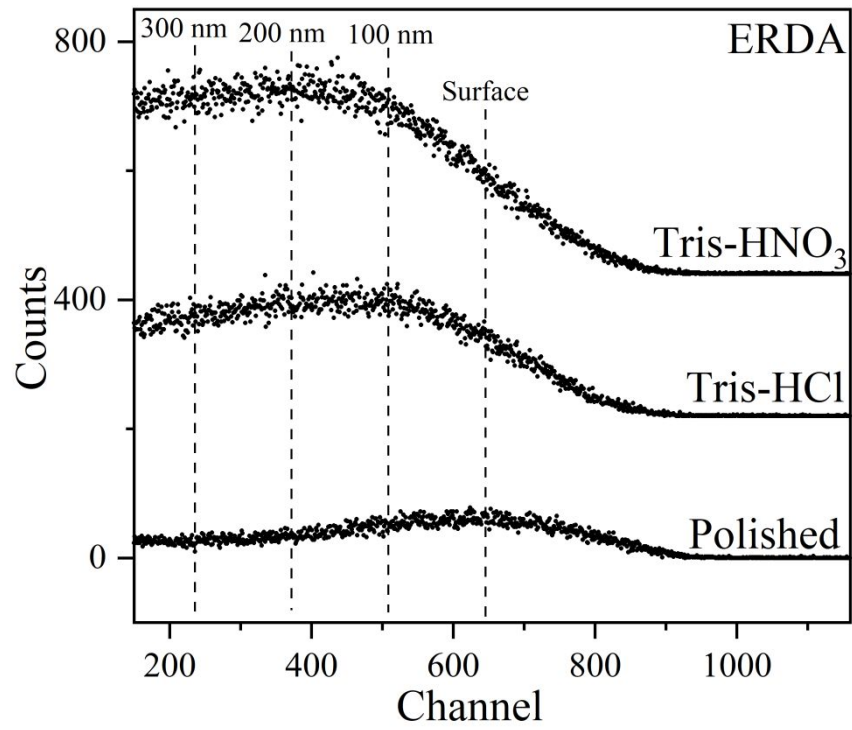


Figure 10

## Tables

**Table 1.** Estimated forward rates of Na, B, and Si for the studied glass in Tris-based solutions.  $N_4$  fraction (%) of the recovered glassy grains after dissolution experiments, as assessed by  $^{11}\text{B}$  MAS NMR studies. For reference to the reader, the initial glass has an  $N_4$  value of 68.2%.

Aqueous Media	Starting pH	Normalized Loss Rates (g-glass/[m <sup>2</sup> h])						$N_4$ (24 h <sup>*</sup> )
		Na	Na-error	B	B-error	Si	Si-error	
0.1 M Tris-HCl	7	47.5	±0.7	46.1	±0.9	12.6	±0.3	70.3
0.1 M Tris-HNO <sub>3</sub>	7	41.1	±5.5	40.6	±5.8	9.4	±2.4	71.3
0.01 M Tris-HCl	8	29.4	±0.6	25.7	±0.7	12.7	±0.2	71.0
0.01 M Tris-HNO <sub>3</sub>	8	23.4	±2.6	20.5	±2.3	9.8	±1.2	70.2
0.05 M Tris-HCl	8	28.3	±0.8	25.3	±0.8	8.8	±0.7	n.d. <sup>†</sup>
0.05 M Tris-HNO <sub>3</sub>	8	24.6	±1.2	24.1	±1.0	8.3	±0.7	n.d.
0.1 M Tris-HCl	8	25.3	±0.4	24.6	±0.4	7.92	±0.03	69.8
0.1 M Tris-HNO <sub>3</sub>	8	24.6	±1.2	24.1	±1.0	8.3	±0.7	69.7
0.3 M Tris-HCl	8	17.4	±1.0	18.4	±1.1	6.8	±0.5	n.d.
0.3 M Tris-HNO <sub>3</sub>	8	18.5	±0.7	19.8	±0.7	6.9	±0.3	n.d.
0.5 M Tris-HCl	8	14.4	±0.6	16.3	±0.7	5.7	±0.5	69.5
0.5 M Tris-HNO <sub>3</sub>	8	14.6	±0.4	16.5	±0.4	5.3	±0.5	69.5
0.1 M Tris-HCl	9	26.7	±2.9	28.8	±3.0	15.1	±3.0	69.1 (12 h)
0.1 M Tris-HNO <sub>3</sub>	9	26.4	±1.3	28.4	±1.5	16.2	±1.1	69.2 (12 h)

\*Unless otherwise noted

†Not determined

**Table 2.** Surface compositions of the studied glass sample as measured in the top 3–10 nm via XPS analysis (atomic percentages accurate within ±5%). We have compared the composition of the polished and dissolved samples to the bulk composition measured using ICP-OES. H concentrations were measured using ERDA analysis.

Element (at. % by XPS)	Bulk	Polished Surface	0.1 M Tris-HCl (pH = 7), 24 h	0.1 M Tris-HNO <sub>3</sub> (pH = 7), 24 h
Na	14.4	13.6	0.7	1.4
B	14.3	9.8	0.0	0.0
Si	14.2	14.7	26.2	25.6
O	57.1	61.8	73.2	73.1
H*	--	<0.1	3.5	5.2

\*H concentration in the top ~350 nm as determined from ERDA (within ±5 %)